Chemical Physics Letters 577 (2013) 38–41

Contents lists available at SciVerse ScienceDirect

Chemical Physics Letters

journal homepage: www.elsevier.com/locate/cplett

Matalon–Packter law for stretched helicoids formed in precipitation processes

Shibi Thomas [a], Ferenc Molnár [b], Zoltán Rácz [c], István Lagzi [d,*]

[a] Department of Physics, University of Calicut, Kerala, India
[b] Department of Physics, Applied Physics, and Astronomy, Rensselaer Polytechnic Institute, Troy, NY, USA
[c] Institute for Theoretical Physics, Eötvös University – HAS, Budapest, Hungary
[d] Department of Physics, Budapest University of Technology and Economics, Budapest, Hungary

ARTICLE INFO

Article history:
Received 29 March 2013
In final form 17 May 2013
Available online 25 May 2013

ABSTRACT

Helicoid-like precipitation structures emerging in the wake of reaction–diffusion fronts are studied experimentally as well as theoretically. We find that the helicoids are stretched, their local pitch behind the advancing front increases exponentially. We compare this result to the exponential increase of the band spacing in Liesegang phenomena. The spacing coefficient (p) characterizing the exponential increase satisfies the same Matalon–Packter law in both cases, i.e. $p \sim 1/a_0$ where a_0 is the initial concentration of the outer electrolyte in the experimental setup. Our experiments also reveal that, at the microstructure level, the helicoids are assembled from building blocks of micron-size achiral spherulites.

1. Introduction

Helical and helicoidal structures are common architectures in nature and in man-made systems such as inorganic crystals or nanohelices [1–5]. The formation of these inherently chiral patterns is an interesting and rather complex problem due to the symmetry breaking which takes place at some stage of their evolution. In our recent work [6] we showed that emergence of helicoids and helices in precipitation processes in the wake of a planar reaction–diffusion front is an intrinsic property of the system and (in contrast to coming from initial and boundary condition effects) it can be attributed to a sophisticated interplay among the noise, the moving front, and the unstable modes of the precipitation dynamics. Our findings reveal that the emergence of helicoidal and helical patterns is reproducible with a finite, well-defined probability depending on the parameters of the system such as the initial concentration of the outer and inner electrolytes, the temperature and the width of the system (see Figures 1 and 2 for the experimental setup). Remarkably, the trends in the observed probabilities could be reproduced by generalizing a model used earlier for explaining Liesegang phenomena [6].

The helicoids and helices are actually closely related to Liesegang patterns which are precipitation patterns emerging in the wake of reaction–diffusion fronts, but the precipitation zones are parallel to each other. The position of the bands, their width, and their time of appearance are well characterized for Liesegang patterns [7–9]. In particular, the distance between consecutive bands in regular Liesegang phenomenon increases as a geometrical series and it can be characterized by the so-called spacing coefficient, p, such that $x_{n+1} - x_n = px_n$, where x_{n+1} and x_n are the positions of two consecutive bands measured from the initial junction point of the electrolytes. This is the well-know spacing law which has been the focus of a large number of studies [8–10]. It has been shown experimentally that the spacing coefficient depends on the initial concentrations a_0 and b_0 of the outer and inner electrolytes, as described by the following relation (Matalon–Packter law) [11,12]:

$$p = f(b_0) + \frac{g(b_0)}{a_0}, \tag{1}$$

where f and g are weakly dependent (decreasing functions) of their arguments.

It is a natural question whether the method of characterization of bands can be extended to helices as well, where the distance between the bands is equivalent to the local pitch of the helices. Our aim with this letter is to suggest that the spacing law and the related Matalon–Packter law are valid for helices. This suggestion is supported by the accord between our numerical simulations and the experimental findings. We also examine the microstructure of precipitation helicoids in order to ascertain that the origin of macroscopic helices is in symmetry breaking and not the chirality of the microscopic building blocks.

2. Experimental

Our experiments concerned the $CuCl_2$ and K_2CrO_4 precipitation reaction in a 1% agarose gel according to the chemical reaction

* Corresponding author. Fax: +36 1 463 1896.
E-mail address: lagzi@vuk.chem.elte.hu (I. Lagzi).

0009-2614/$ - see front matter © 2013 Elsevier B.V. All rights reserved.
http://dx.doi.org/10.1016/j.cplett.2013.05.031

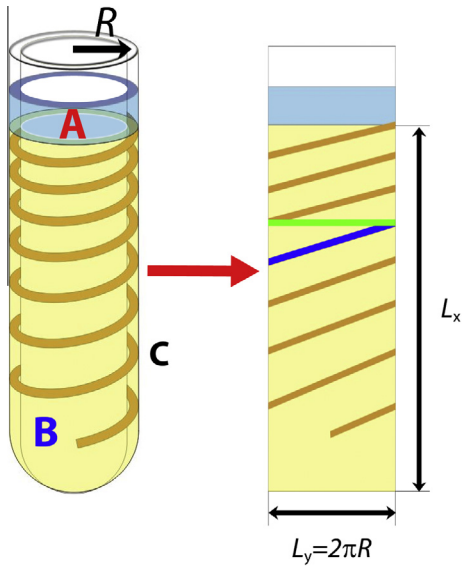

Figure 1. Transformation of the 3D experimental setup into a 2D domain used in numerical simulations. The unfolding of the cylinder onto the 2D domain ($L_x \times L_y$) requires that the boundary conditions are periodic in the horizontal direction, and the width of the domain L_y is defined by the radius R of the cylinder: $L_y = 2\pi R$. The single brown line (C) of helix in 3D corresponds to a set of tilted precipitation zones (lines) joined by the periodic boundary condition. Blue and yellow colors mark the regions where the reagents (A – outer electrolyte, B – inner electrolyte) are placed initially. (For interpretation of the references to colour in this figure legend, the reader is referred to the web version of this article.)

$Cu^{2+}(aq) + CrO_4^{2-}(aq) \rightarrow CuCrO_4(s)$ [13]. Agarose gel in a test tube contained potassium chromate as inner electrolyte was prepared by dissolving potassium chromate (K_2CrO_4, Sigma–Aldrich – the inner electrolyte) in double distilled water with the given amount of agarose powder (Type I, Sigma–Aldrich). The mixture was heated to 90 °C under constant stirring until a homogeneous solution was obtained. The resulting solution was then poured into test tubes of 16 mm diameters. After polymerization (2 h) a solution of copper chloride ($CuCl_2$, Sigma–Aldrich – the outer electrolyte) was gently poured on top of the potassium chromate-doped gel (see Figure 1 for the experimental setup). The pattern formation was monitored at room temperature (22.0 ± 0.3 °C) by a digital camera for 7 days. All experiments were carried out with much higher concentrations of the outer electrolyte ($CuCl_2$). Details of the experimental parameters used are described in Ref. [13]. Experimental results indicate that both the Liesegang bands and the helicoids/helices emerge in a wide range of the parameters. In general, we found that precipitation helicoids formed with higher probability when the concentration of the outer electrolyte was higher, thus ensuring fast motion of the front [6]. Noise (e.g., thermal) also plays a crucial role in helicoid formation, probability of the emergence of helicoids increases with the amplitude of the noise. Finally, the radius of the test tube also has the influential effect. The probability of helicoidal pattern formation increases with the radius of the test tube. Moreover, there is a critical radius, below which only Liesegang bands are formed regardless of the other parameters.

3. Numerical

Models of Liesegang phenomena use various aspects of pre- and post-nucleation dynamics. A theory that incorporates both dynamics through a phase separation scenario is based on the Cahn–Hilliard equation [14]. This description features fast, spinodal-decomposition type precipitation dynamics, as well as slower, nucleation-and-growth processes [15] and it can reproduce all the well-established laws related to Liesegang patterns (time-, spacing-, width-, and Matalon–Packter laws) [8–12].

We use the Cahn–Hilliard dynamics combined with reaction–diffusion equations which produce the reaction front where the particles for the precipitation are produced. Assuming an irreversible reaction A + B → C between the outer (A) and inner (B) electrolytes, the pattern formation phenomena in the gel is described by the following reaction–diffusion equations

$$\partial_t a = D\Delta a - kab \tag{2}$$

$$\partial_t b = D\Delta b - kab \tag{3}$$

$$\partial_t m = -\lambda\Delta\left(m - m^3 + \sigma\Delta m\right) + kab + \eta_c, \tag{4}$$

where k is the reaction rate and, for simplicity, the diffusion coefficients (D) of the reagents are taken to be equal. m is the shifted and appropriately scaled concentration of the precipitating particles (C). The front is described in terms of the spatio-temporal properties of kab (rate of production of C's), and λ, σ, η_c are the rescaled kinetic coefficient, surface tension, and conserved noise, respectively [6,16]. During the precipitation process the C particles segregate into low (c_l: m = −1) and high (c_h: m = 1) concentration states described by Eq. (4) (for the detailed model description see Refs. [6,16]). Eqs. (2)–(4) were solved by applying a 'method of lines' using spatial discretization on a rectangular grid followed by integration of the resulting ordinary differential equations by the forward Euler method. The conserved noise η_c was realized by moving Cs to neighboring sites at a rate $\eta_c = r\sqrt{\bar{c}}$, where r is a random number uniformly distributed in an interval $[-\eta, \eta]$ with η characterizing the strength of the noise. The grid spacing and the time step were 1.0 and 0.02, respectively. We used periodic boundary conditions in the y direction (see Figure 1 for the reason of periodicity) and no-flux boundary conditions at the lower edge of the gel ($x = L_x, y$). The boundary condition at the upper edge ($x = 0, y$) for A is a Dirichlet boundary, according to the assumption that the concentration of the outer electrolyte is kept at a constant value $a(x = 0, y, t) = a_0/\bar{c}$, while Neumann (no-flux) boundaries are used for B and C. The outer electrolyte concentration (a_0) was scaled by $\bar{c} = (c_h + c_l)/2$ in both experiments and numerical simulations. As can be inferred from Figure 1, parallel zones and tilted lines in simulations correspond to regular Liesegang and helical patterns, respectively. Solving the above numerical model with various initial and external parameters allowed us to characterize the spacing coefficient of helices and to compare these data with the experimental findings.

4. Results and discussion

In our experiments, helicoidal patterns emerged in columns of gel placed in test tubes. In this setup a planar diffusion front of the outer electrolyte moves into the gel and, in general, produces a series of distinct precipitation disks which is called the regular Liesegang pattern (see Figure 2). However, using the same experimental conditions, helicoidal pattern can also evolve (with well-defined probability) showing the stochastic nature of this phenomenon. In order to compare the properties of regular and helicoidal patterns, we carried out at least 10 independent experiments at the same fixed parameters and conditions.

To investigate the Matalon–Packer law for the helicoids we need to generalize the concept of spacing coefficients for helices. This can be done by defining x_n through the position of the nth crossing of the helix at a given y (Figure 2), and then $x_{n+1}/x_n - 1 = p_n$ should converge to the spacing coefficient p for large n (plotting x_{n+1} versus x_n and determining the slope of fitted linear curve). Note, that helices are often characterized by their pitch. It

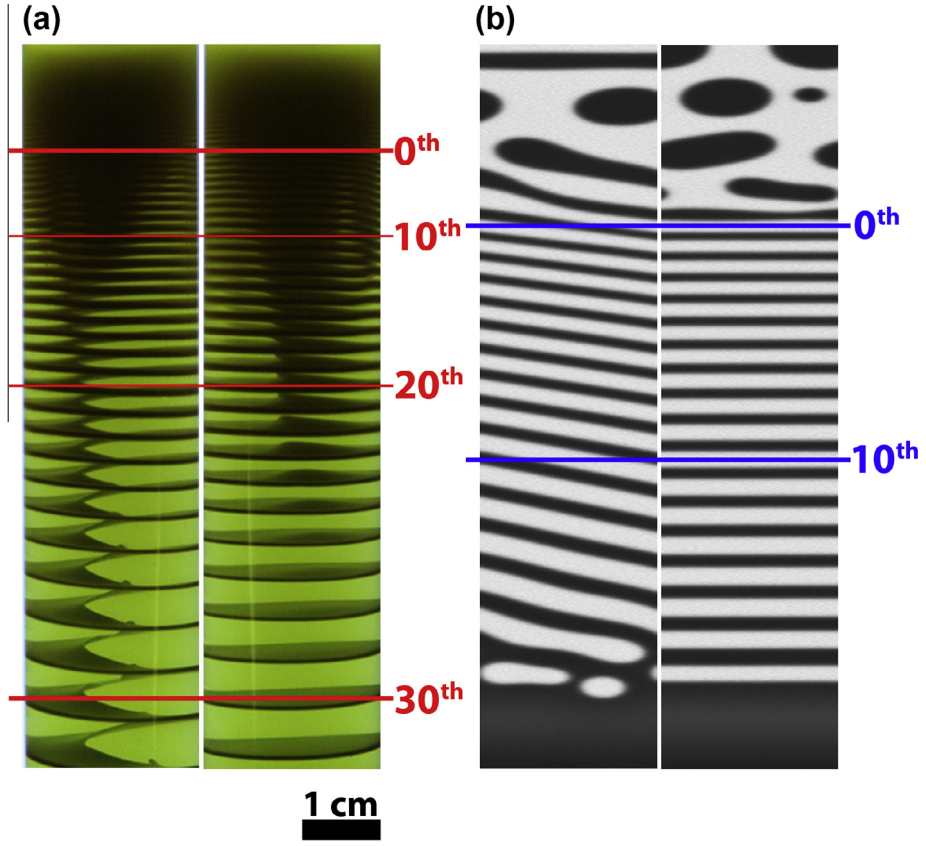

Figure 2. Visual demonstration of the near equality of the spacing parameters for helicoids and for regular Liesegang bands. The patterns were grown experimentally (a) and numerically (b) in identical circumstances. Experimentally, we used $[Cu_2^+]_0 = a_0 = 0.5$ M, and $[CrO_4^{2-}]_0 = b_0 = 0.01$ M, while the scaled parameters in numerical simulations were $a_0 = 80.0$, $b_0 = 1.0$, $\sigma = 0.8$, $\lambda = 0.2$ and $\eta = 0.007$.

is clear from both the experiments and simulations (Figure 2) that the pitch of the Liesegang helices increases as the distance from the initial junction of the electrolytes increases. Only a local pitch $q_n = x_{n+1} - x_n$ can be defined which can be expressed through the spacing coefficient as $q_n = x_{n+1} - x_n = px_n$.

Figure 3 displays the dependence of the spacing coefficient as a function of $a_0/\bar{c}$ for both bands and helices obtained in experiments as well as in simulations [6]. The experimental results for

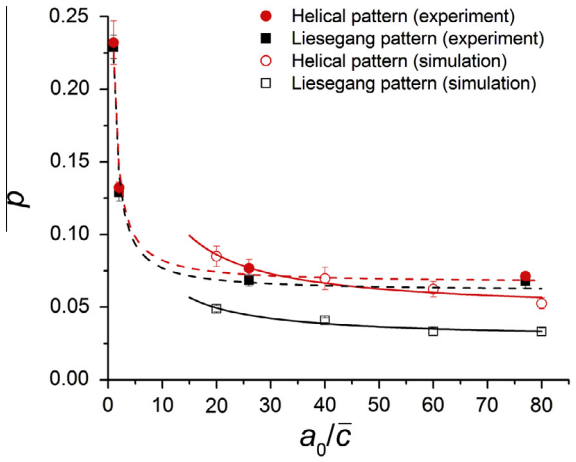

Figure 3. Dependence of the spacing coefficient, p, on the scaled initial concentration of the outer electrolyte, $a_0/\bar{c}$ (copper chloride in experiments). The lines represent the fitted function $p = c + d/a_0$ showing that the Matalon–Packter law is equally valid for precipitation bands and helices.

helices and bands are close to each other with the helices having slightly larger spacing coefficients. Since the data for both the regular bands and helices follow the same curves and can be fitted well to the form of Eq. (1), we conclude that not only the band spacing but also the local helical pitch follows the Matalon–Packter law. As to the simulations, we can select parameter values so that the spacing coefficients are roughly equal to the experimental values, but due to the low probability for the emergence of helices we could not explore the small $a_0/\bar{c}$ range. Nevertheless, in the available interval $(20 < a_0/\bar{c} < 80)$ the simulation results can be well fitted to the Matalon–Packter law.

An observed feature of both the simulations and the experiments is that the local pitch of the helices is always slightly larger than the local band spacing of the Liesegang patterns obtained with the same setup. The difference can be explained if we assume that the bands and the helices have the same local concentrations of the precipitate and the same local widths. Indeed, since the front leaves behind a constant concentration of C's [12] which are collected into a band or a helix (tilted band), it follows that the amount of precipitate in a band (see the green band in Figure 1) is always smaller than that in the corresponding part of the helix (see tilted blue band in Figure 1). Thus, it can be concluded that the pitch of the helix must be larger than the band spacing in order to collect the same amount of C's.

Finally, we mention an additional outcome of our experiments related to the origins of formation of helicoidal structures. The pattern formation process may proceed along two routes. First a template may transcribe a micro- or mesoscopic originally helical structure (e.g., agrogel fibers) onto new structure at higher level (e.g., inorganic crystal) [17]. A distinct possibility, however, is the symmetry breaking route where building blocks having no

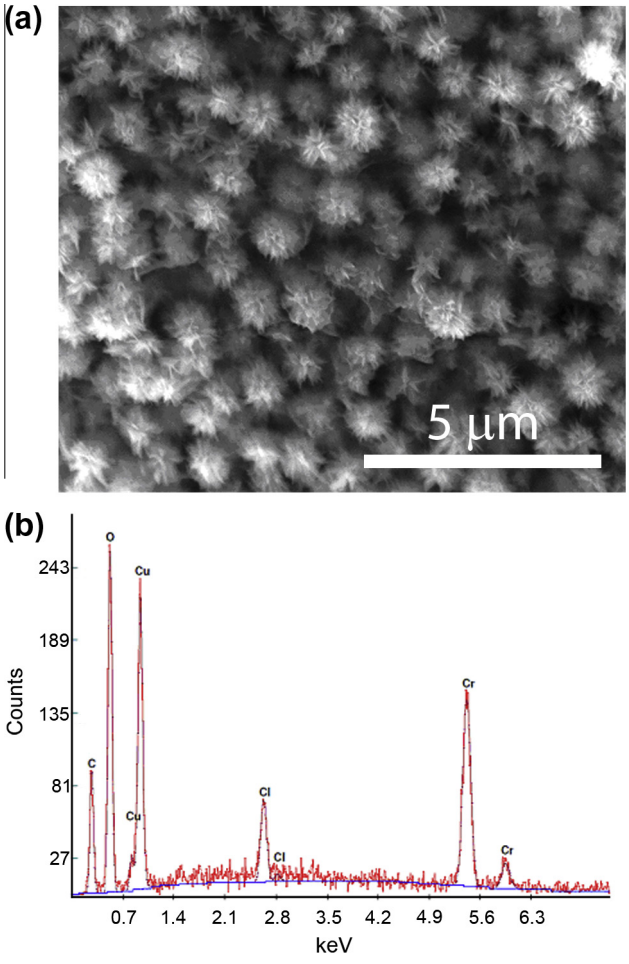

Figure 4. SEM micrograph (a) and the EDS spectrum (b) of the copper chromate microcrystals from a precipitation helicoid in a 1% agarose gel. The building blocks are spherulites showing no chirality at this microscopic level.

chirality self-organize into highly ordered right- and left-handed helical/helicoidal structures [2,18]. The usual argument for emergence of crystals with chiral morphology at micrometer scale is a twisted assembly of achiral blocks driven by mass transport. In these structures the diameter of the helices is comparable to the size of the achiral building blocks [2,18]. We used SEM to investigate the microstructure (building blocks) of helical patterns, and we found that the precipitation helicoid consists of monodisperse spherulite-like particles of ~1 μm size (Figure 4). These building blocks appear to be achiral, thus we believe, the macroscopic helicoids, which have four orders of magnitude larger size, emerged as a result of symmetry breaking, and not as a result of the microscopic chirality magnified to the macroscopic level.

5. Conclusions

The main aim of this study was to investigate dependence of spacing coefficient of helicoidal and helical patterns on the initial concentration of the outer electrolytes in a precipitation system. Based on experimental and numerical results we were able to quantify this dependence, and we could conclude that the Matalon–Packter law is valid for precipitation helicoids as well. We found that such chiral precipitation helicoids are made of building blocks of achiral crystallites of 1 μm size. We believe that understanding of helicoidal and helical patterns in reaction–diffusion systems is important since it may help in designing and engineering similar helicoidal and helical structures in other chemical and physical systems (e.g., frontal polymerization, alloy systems), which could have unique physical and chemical properties.

Acknowledgments

Authors acknowledge the financial support of the Hungarian Research Found (OTKA K81933, K77908, K104666, and NK100296) and the Zoltán Magyary Postdoctoral Fellowship and the European Union and the European Social Fund (TÁMOP 4.2.4.A-1). F.M. acknowledges partial support by the NSF through Grant No. DEB-0918413.

References

[1] P.X. Gao, Y. Ding, W.J. Mai, W.L. Hughes, Z.L. Wang, Science 309 (2005) 1700.
[2] H. Imai, Y. Oaki, Angew. Chem., Int. Ed. 43 (2004) 1363.
[3] S.C. Müller, S. Kai, J. Ross, Science 216 (1992) 635.
[4] R.V. Suganthi, E.K. Girija, S.N. Kalkura, H.K. Varma, A. Rajaram, J. Mater. Sci. Mater. 20 (2009) 131.
[5] O. Giraldo, S.L. Brock, M. Marquez, S.L. Suib, H. Hillhouse, M. Tsapatsis, Nature 405 (2000) 38.
[6] S. Thomas, F. Molnár, I. Lagzi, Z. Rácz, Phys. Rev. Lett. 110 (2013) 078303.
[7] R.E. Liesegang, Naturwiss. Wochenschr. 11 (1896) 353.
[8] H.K. Henisch, Crystals in Gels and Liesegang Rings, Cambridge University Press, Cambridge, 1988.
[9] S.C. Müller, J. Ross, J. Phys. Chem. A 107 (2003) 7997.
[10] K. Jablczynski, Bull. Soc. Chim. Fr. 33 (1923) 1592.
[11] R. Matalon, A. Packter, J. Colloid Sci. 10 (1955) 46.
[12] T. Antal, M. Droz, J. Magnin, Z. Rácz, M. Zrinyi, J. Chem. Phys. 109 (1998) 9479.
[13] I. Lagzi, Langmuir 28 (2012) 3350.
[14] T. Antal, M. Droz, J. Magnin, Z. Rácz, Phys. Rev. Lett. 83 (1999) 2880.
[15] E.T. Gawlinski, J. Vinals, J.D. Gunton, Phys. Rev. B 39 (1989) 7266.
[16] A. Volford, I. Lagzi, F. Molnár, Z. Rácz, Phys. Rev. E 80 (2009) 055102(R).
[17] J.H. Jung, Y. Ono, K. Hanabusa, S. Shinkai, J. Am. Chem. Soc. 122 (2000) 5008.
[18] Y. Oaki, H. Imai, J. Am. Chem. Soc. 126 (2004) 9271.